Physica Scripta

PAPER

Ab initio prediction of half-metallic and metallic ferromagnetism in ZnO:(Co,Cr) systems

RECEIVED
10 February 2024

REVISED
6 April 2024

ACCEPTED FOR PUBLICATION
25 April 2024

PUBLISHED
7 May 2024

V N Jafarova[1], **U S Abdurahmanova**[2] **and S S Rzayeva**[3]

[1] Department of Physics, Azerbaijan State Oil and Industry University, 20 Azadlig Ave., Az-1010, Baku, Azerbaijan
[2] Baku Engineering University, Khirdalan city, Hasan Aliyev str., 120 AZ-0101, Absheron, Azerbaijan
[3] Azerbaijan State University of Economics, 6 Istiglaliyyat Str., AZ-1001, Baku, Azerbaijan

E-mail: vcafarova@beu.edu.az

Keywords: ZnO structure, magnetic properties, magnetic moment, metallic, half-metallic

Abstract

Doping effects on the electronic and magnetic properties of $Zn_{1-x}(Co,Cr)_xO$ systems are investigated within Local Spin Density Approximation and Hubbard U methods. Based on Density Functional Theory the spin-polarization band structures, density of states for investigated systems are calculated. Systematic analysis of the electronic properties shows that TM-doped ZnO has generated new energy levels in the vicinity of Fermi energy level. From first-principle calculations we obtained Cr-ZnO and Co-ZnO systems are metallic and half-metallic ferromagnetic materials, respectively. The obtained results for Cr-doped ZnO 128- and 192-atom supercell systems show magnetic properties with higher Curie temperature than room temperature. There are large local moments, ~2.9 and ~4.2 for Co and Cr dopants, respectively. Magnetic moments are related with two electron defects in the supercell structure and unpaired electrons of transition metal. The ferromagnetic and antiferromagnetic phases and the total energy are obtained for $x = 2.08\%$, 3.125%, 4.16%, 6.25%, 8.3%, 12.5%, and 25% impurity concentrations for doped ZnO.

1. Introduction

In recent years, DMS materials have given an opportunity to the development of spin-based devices with potential to run at sufficiently high speeds while consuming less energy than conventional devices. These compounds enable the production of new types of materials with the most substantial technological applications in optoelectronics and spintronics.

The II-VI semiconductor group oxide materials are one of the most important and interesting compounds, having promising technical possibilities in different fields for the reason that of their large energy gap [1–4] and considered between the best DMSs. Room temperature ferromagnetism (RTFM) and higher Curie temperature in dilute magnetic oxides is the most possible new issue in magnetism. The diluted magnetic oxide materials are applied in spintronics only if additional impurities are introduced. The transition metal doped oxide materials exhibit both ferromagnetism and semiconducting properties. The 3d TM-doped systems have great research interest by scientists and researchers as efficient applicants for a new generation for spin-based devices. These type magnetic semiconductor materials are used to make quantum computing architecture employmenting spin-polarized electrons and in magneto optic applications.

The investigated pure ZnO layered semiconductor has nonmagnetic properties. ZnO has great potential in the field of production of piezoelectric transducers, optical devices, solar cells, sensors etc [5–14]. It could be used in spintronic devices only if additional dopants are introduced in this structure. Zinc oxide can manage as a semi-metallic property and is a useful material for producing spin-based devices.

The defect engineering of the ZnO has remained an important motivation in materials science research as the fundamental physical and chemical properties of ZnO much depend on their defect structures. It is because of the complex nature of the defects that ZnO is being discovered and rediscovered repeatedly. Among the nonmagnetic oxides such as TiO_2, SnO_2, and In_2O_3, because ZnO has large energy gap ($E_g = 3.4$ eV) and higher

binding energy ($E_b = 60$ meV) at room temperature (RT), because of which the excitonic emission processes persist at or even above RT. Due to these properties Zn-based diluted magnetic oxides have attracted great research interest in recent years [15–17]. This exceptional characteristic feature makes it a remunerative material for RT ultraviolet (UV) lasing devices. It acts as a potential candidate for application in optoelectronic and spintronic devices. The material properties of ZnO make it applicable to a wide range of applications in UV light emitters, varistors, ceramic positive temperature coefficient thermistors, transparent high-power electronics, surface acoustic waveguides, piezoelectric transducers, chemical and gas sensing, solar cells, piezoelectric nanogenerators (PNGs), etc [18–22].

Most of the previous theoretical studies have been obtained a smaller band gap than the experimental value (3.37 eV) for ZnO wurtzite crystals, despite using the Hubbard U semiempirical corrections [23]: 1.245 eV (U_d (Zn) = 15 eV) [24], 2.286 eV (U_d (Zn) = 10; U_p (O) = 9 eV) [25] and 0.945; 1.062; 1.154 eV (U_d (Zn) = 2; 4; 6 eV) [26], using GGA + U and LDA + U methods, respectively. In the present work, we have been obtained that the first-principle calculated energy gap using LDA and GGA approximations of ZnO is 0.7 and 0.67 eV, respectively, which is smaller than the known experimental value. Then we have been able to reproduce the experimental value of the energy gap of ZnO crystal only using Hubbard U corrections [23] in our calculations. The calculated band gap for bulk ZnO correspondingly previous experimental values is reported by *ab initio* calculations using LDA (GGA) + U [23] method. Note that the value of U hasn't any significant effect on the structural properties of investigated systems [27].

Sato *et al* [28] predicted that TM-doped ZnO may be a ferromagnetic material. Krishnan *et al* [29] and Li *et al* [30] found room temperature ferromagnetism with higher Curie temperature in ZnO:Cr systems synthesized by magnetron sputtering experiment. Venkatesan *et al* [31] reported the results of magnetic behavior of ZnO:(Co, Cr) systems with 5% impurity concentrations, and room temperature FM phase is observed in Co-doped ZnO film and found 2.6 μ_B magnetic moment for impurity atoms. Ueda *et al* [32] show that ZnO:Co thin films with a few impurity concentrations exhibit FM phases with a higher Curie temperature. Najim *et al* [33] found RTFM behavior for Cr-doped ZnO sample and estimated the magnetic moment is 2.8 μ_B/Cr, and obtained result for magnetic moment ~1 μ_B/Cr less than the calculated value [34]. It is known that the FM behavior of DMS compounds also depends on the technology of synthesis of these materials. In other experimental works, Roberts *et al* [35] and Li *et al* [34] found that the values of magnetic moments were ~1.4 and ~0.58 μ_B/Cr (1.2%); ~0.14 μ_B/Cr (with $x = 6.7\%$).

The purpose of this study is to investigate the underlying magnetic mechanisms of ZnO-based DMSs, hence ZnO:(Co,Cr) systems with a low impurity concentration were built. This paper is devoted to analyzing of electronic and magnetic properties in TM (Co^{2+}, Cr^{2+}) ions doped $Zn_{1-x}M_xO$ systems with concentrations of $x = 2.08\%$, 3.125%, 4.16%, 6.25%, 8.3%, 12.5% and 25%. For both doped systems the Curie temperatures are estimated to investigate the technical application possibilities. The interpretation of the results of total density of states (TDOS) shows the metallic FM behavior of ZnO:Cr with the band gap of 0 eV. The magnetic moments of Co-ZnO and Cr-ZnO DMSs are 3 and 4 μ_B, respectively. The $Cr_xZn_{1-x}O$ system is high Curie temperature metallic ferromagnetic DMS material for new-generation spintronic devices. ZnO:Co is a very good choice for electronic devices due to its low Curie temperature.

2. Simulation method

First-principles simulations carried out implementing the Atomistic ToolKIt (ATK) code (http://quantumwise.com/) and this is a software for atomic-scale modeling and simulation of nanosystems. ATK combines density functional theory (DFT) with non-equilibrium Green's functions for first-principles electronic structure and transport calculations of molecules, periodic systems etc. DFT is infamous for foretelling very small band gaps. It is well known that local density approximation (LDA) functional generally underestimate band gaps and that hybrid DFT or self-interaction corrected calculations correct these issues more universally in most systems. In [21] the authors reported that the band gaps of various periodic systems can be generally improved with DFT methods using HSE06 range-separated hybrid functionals and Wannier-Fermi-Lo ¨wdin self-interaction corrections. Nevertheless, the last progress of LDA functional and using Hubbard U semiempirical corrections have given us an opportunity to determine correct band gaps of materials.

In our DFT calculations, to simulate the $Zn_{1-x}Co_xO$ and $Zn_{1-x}Cr_xO$ 32-, 48-, 64-, 96-, 128- and 192-atoms supercells with impurity concentrations of $x = 2.08\%$, 3.125%, 4.16%, 6.25%, 8.3%, 12.5% and 25% were used. For this purpose single and double Zn in structures were replaced by dopants. The interaction between electron and ion is taken into account by the ionic pseudopotentials of the Fritz-Haber-Institute (FHI) [36]. The exchange correlation effects between structure atoms are processed in the form of Perdew Zunger (PZ) functional [37] under the local spin density approximation (LSDA). The kinetic cutoff of energy for plane waves was taken about 50 Ha was employed throughout the calculations which were tested to be fully converged with

for total energy. The calculation convergence criterion in the case of the optimization of supercell structures containing Co and Cr atoms were relaxed and geometrical optimized due to no higher than 0.01 eV/Å force and 0.01 eV Å^3 stress tolerances. The reciprocal space integration was performed using $5 \times 5 \times 5$, $3 \times 2 \times 3$, $2 \times 2 \times 2$, and $2 \times 1 \times 2$ for 32- (or 48-), 64-, 96- (or 128-), and192-atom supercells Monkhorst–Pack (MP) k-sampling grids [38]. Note that, for all calculations, the convergence of the plane-wave basis set cutoff energy and Brillouin zone integration k-point sampling of ZnO were tested. The 12 electrons for Zn [Ar] + $3d^{10}4s^2$, 6 electrons for O [Ar] + $4s^2 4p^4$, 9 electrons Co [Ar] + $3d^7\ 4s^2$, and 6 electrons for Cr [Ar] + $3d^5\ 4s^1$ were taken as the valence electrons. By successfully correcting the electronic band structure of the investigated compounds using Hubbard U semiempirical correction, can future extend the study of magnetic properties of doped systems. In this study, applying the Hubbard U correction to solve the band gap problem is necessary for predicting the properties of GaN bulk material. Hubbard correlation energy values were used for zinc 3d- (U = 4 eV) and 4s-states (U = 4.5 eV), and for oxygen 2p-states (U = 3.7 eV). The Hubbard U correction is applied using the simplified approach according to Dudarev *et al* [39], which corresponds to the case $J = 0$ in the more elaborate expression by Lichtenstein *et al* [40].

For the building of the crystal structure of ZnO we have taken the initial structural parameters $a = b = 3.2495$ Å, $c = 5.2069$ Å, and $u = 0.345$ [41].

Using Mulliken population analysis we computed the values of magnetic moments of 3d metal-doped ZnO supercell systems. The Mulliken population analysis has been performed to obtain the occupation number of each atom orbital. Thus the magnetic moments are defined as the difference of occupation number between the spin-up and spin-down states. The partial density of states of the spin is obtained by expanding each discrete energy level according to the Lorentzian formula (1) [42]

$$D^{\alpha}_{nl\sigma}(E) = \sum_i A^{\alpha}_{nl\sigma i} \frac{\delta/\pi}{(E - \varepsilon_{i\sigma})^2 + \delta^2} \tag{1}$$

where i and σ are the indexes of energy level and spin, respectively, $A^{\alpha}_{nl\sigma i}$. is the Mulliken population of atomic orbital of atom α. The total density of states of the spin is defined as the sum of the partial density of states

$$D_{\sigma}(E) = \sum_{nl\alpha} D^{\alpha}_{nl\sigma}(E) \tag{2}$$

For the studying the ferromagnetic (FM) and antiferromagnetic (AFM) spin ordering for the Co-ZnO and Cr-ZnO systems, cations were replaced by $M^{\uparrow}_{x/2}$; $M^{\uparrow}_{x/2}$ and $M^{\uparrow}_{x/2}$; $M^{\downarrow}_{x/2}$ (M = Co, Cr) ions.

The supercell structures with different concentrations of impurities were used to investigate the influence of doping effects on the electronic and ferromagnetic properties in comparison with the un-doped systems.

3. Results and discussion

3.1. Electronic properties of pure ZnO

Investigated material zinc oxide (ZnO) that crystallizes in the wurtzite (hexagonal) structure and possesses C_{6v}symmetry. The electronic band structure of this compound exhibits a splitting of the valence bands at the Γ symmetry point on the center of Brillouin zone due to some effects. In the band structure of ZnO, the conduction band is treated by the $4s^2$ orbitals of zinc having s-like nature, and the top of the valence band is generated by the $2p^4$ electrons of oxygen with p-like nature. To obtain a more accurate electronic structure we implemented Hubbard energy corrections for O p- (3.7 eV), Zn d- (4 eV) and s-states (4.5 eV). We plot in figures 1 and 2 the spin polarized band structures of pure ZnO wurtzite and supercell structures by DFT-LSDA + U method. In these figures the red and black bands describe the down and up-spin band structures for investigated materials. Using the LSDA and Hubbar U approach, we computed the electronic structure for undoped systems and we obtained the gap energy value of $E_g = 3.30$ eV, and this result is in a good agreement with known experimental works [1, 2]. Then we have repeat this structure and built the ZnO supercells with different impurity concentrations.

For pure ZnO, the both up- and down-spin DOS diagrams are identical (figures 3 and 4) and this result indicates that the undoped system is nonmagnetic material. The negative and positive values of density of states are corresponding to the down- and up-spin states.

From first-principles band structures and DOS calculations for un-doped bulk systems, we obtained that the valence bands consist of three parts: lowest valence bands (from –17.8 to –17 eV) are derived from O 2s orbitals. Second (middle) part of the valence bands (from –8.4 to –7 eV) formed mainly by Zn d-states. The top of valence bands with the range from –6.3 to –1.7 eV is mainly treated by O 2p levels. The minimum of the conduction bands is mainly derived by zinc 4s orbitals. Our results show that the valence band maximum and conduction band minimum are located at the Γ point, this fact express that the ZnO is a direct band gap compound.

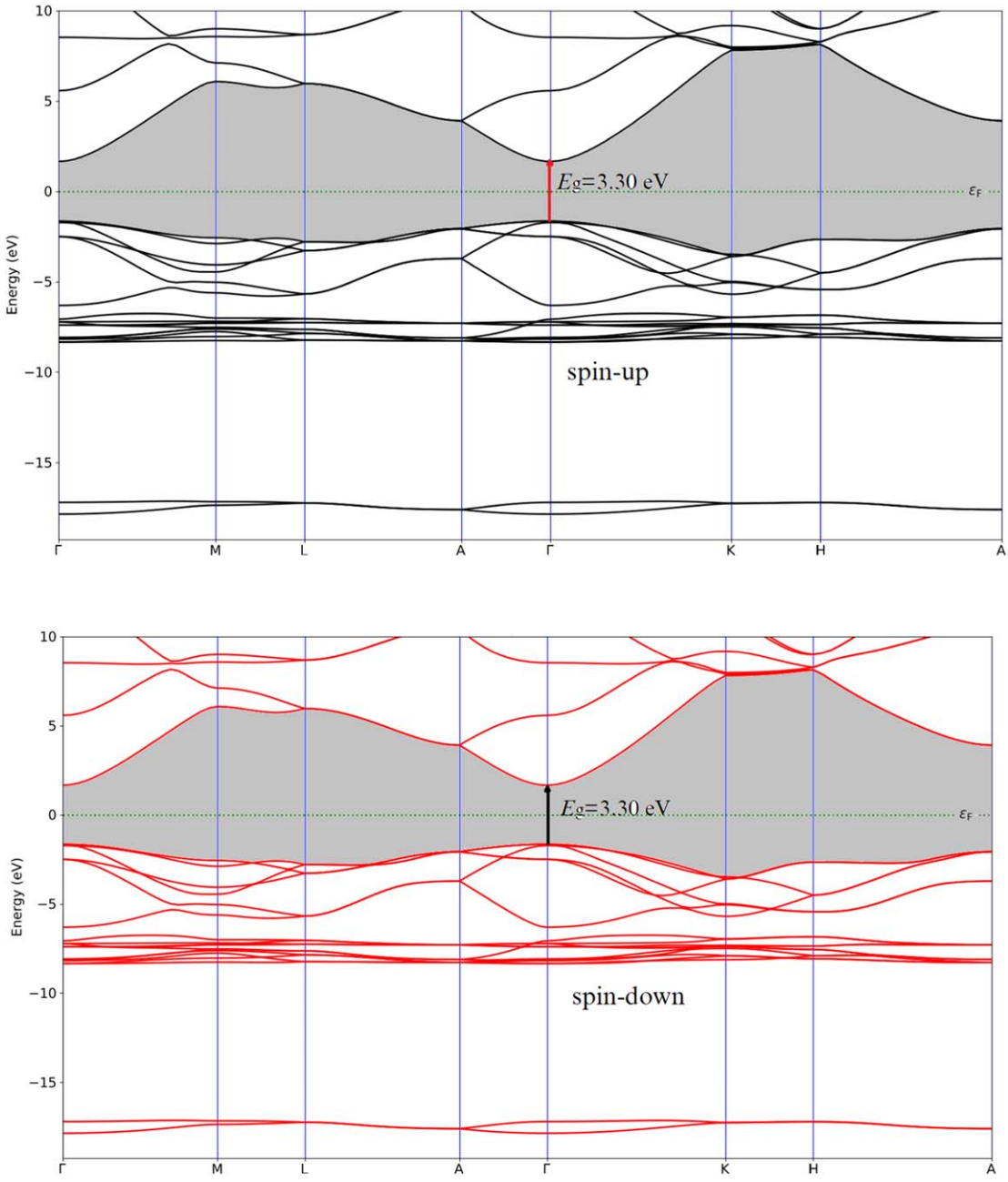

Figure 1. Spin polarized band structures for undoped bulk ZnO with LSDA + U.

3.2. Electronic properties of Co-ZnO

In this section, we will analyze the details of the electronic properties of ZnO doping with different Co concentrations. For the interpretation of the effect of doping concentration, we built 16-, 32-, 48-, 64-, 96-, 128, and 192-atom supercell structures and replaced one or two Zn atoms with cobalt, corresponding to 2.08%, 3.125%, 4.16%, 6.25%, 8.3%, 12.5% and 25% impurity concentrations. Using Mulliken Population analysis we computed the values of local and total magnetic moments of Cr-ZnO defected systems.

We plot in figure 5 the spin-polarized electronic structures of Co-ZnO 8-atom supercell structure by DFT-LSDA + U method. In these figures the red and black bands describe the down- and up-spin structures for Co-ZnO. While two 3d transition metal Co atoms are incorporated, the spin polarized TDOS diagrams are significantly changed near the Fermi energy. In figures 6 and 7, we illustrate the DOS diagrams of Co-ZnO systems. The Fermi energy is set to zero and shown by the horizontal and vertical dotted lines. Note that, in the all DOS diagrams the negative and positive values correspond to the down- and up-spin states.

As seen from figure 6, the Co doping in ZnO has generated new energy levels in the energy gap, resulting in a semi-metallic character of the defected system. As seen from figure 6, near the Fermi energy level the total

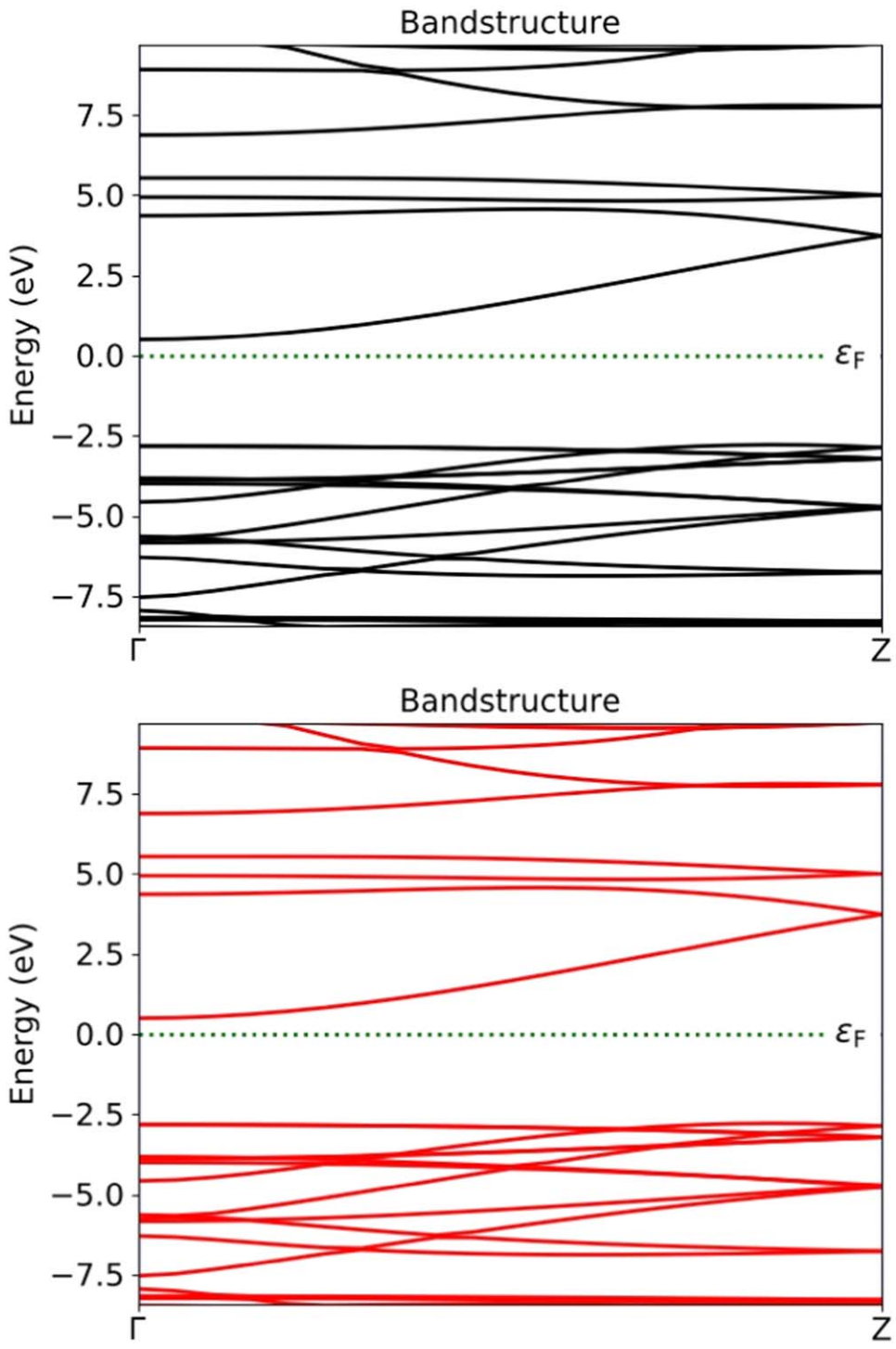

Figure 2. Spin polarized band structures (black-spin-up, red-spin-down states) for undoped ZnO supercell structure with LSDA + U.

density of spin-up and spin-down states for Co-doped ZnO systems, is clearly asymmetrical, which indicates the presence of magnetism in the diluted systems.

First-principles obtained band gap results for different Co-doped ZnO systems are shown in table 1.

As seen figures 5 and 6, we obtained that the Co-doped ZnO compound is half-metal material with narrow energy gaps from 1.2 eV to 3.0 eV and from 0.29 eV to 1.8 eV corresponding to up- and down-spin states. From table 1, we observed an increase of band gaps with a reduction of Co concentration.

3.3. Electronic properties of Cr-ZnO

In this section, we give the first-principles study of the spin polarized electronic structures, DOS diagrams for Cr-ZnO supercell structures with different concentrations of dopants. First-principles obtained band structures

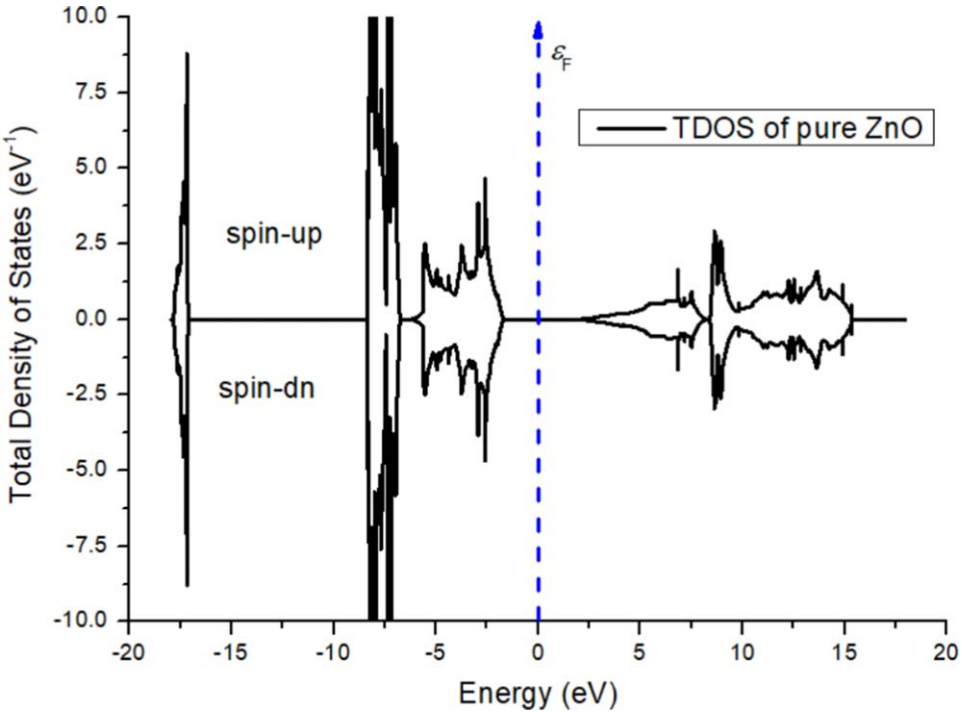

Figure 3. Spin-polarized TDOS of un-doped ZnO bulk wurtzite structure with LSDA + U.

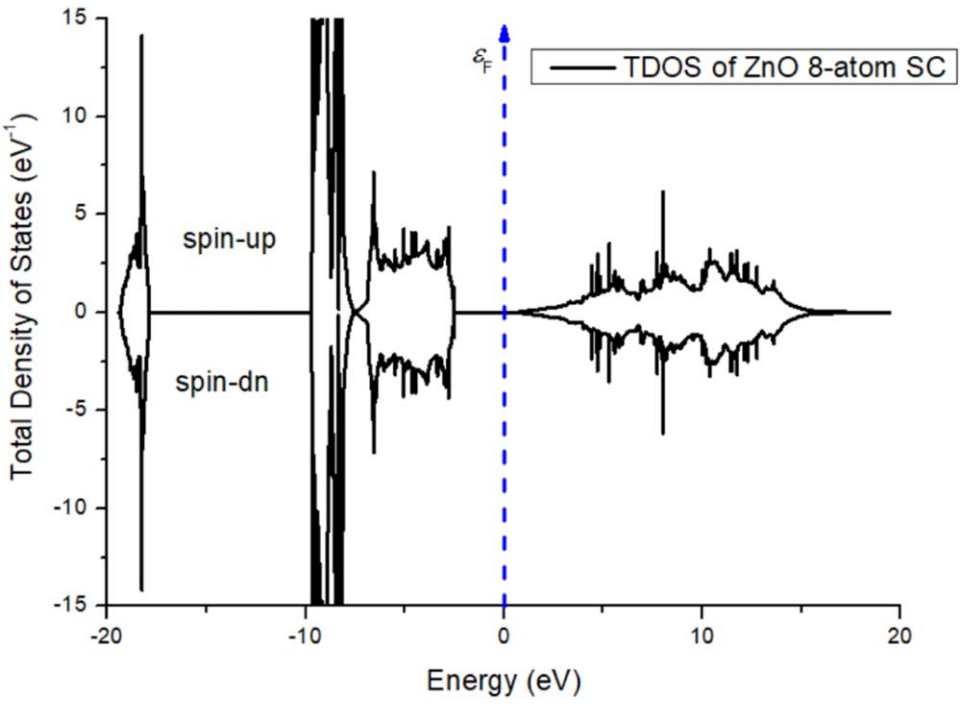

Figure 4. Spin-polarized TDOS for un-doped ZnO 8-atom supercell structure with LSDA + U.

correspond to up- and down-spin states, total and partial DOS diagrams are shown in figures 8–10, respectively. The black and red bands describe the majority and minority spin states for ZnO:Cr systems.

Figures 9 and 10 show that the introduction of Cr atoms in ZnO systems changes the band structures, and some impurity levels occur near the Fermi level. Due to this reason, the up- and down-spin band gaps narrow and these systems show semiconducting character with narrow energy gaps. The DOS calculations for Cr-ZnO systems show some imbalances, especially oxygen *p*- and chromium *d*-orbitals. We observed *pd* hybridization between 2*p*-orbitals of oxygen and 3*d*-orbitals of chromium atoms.

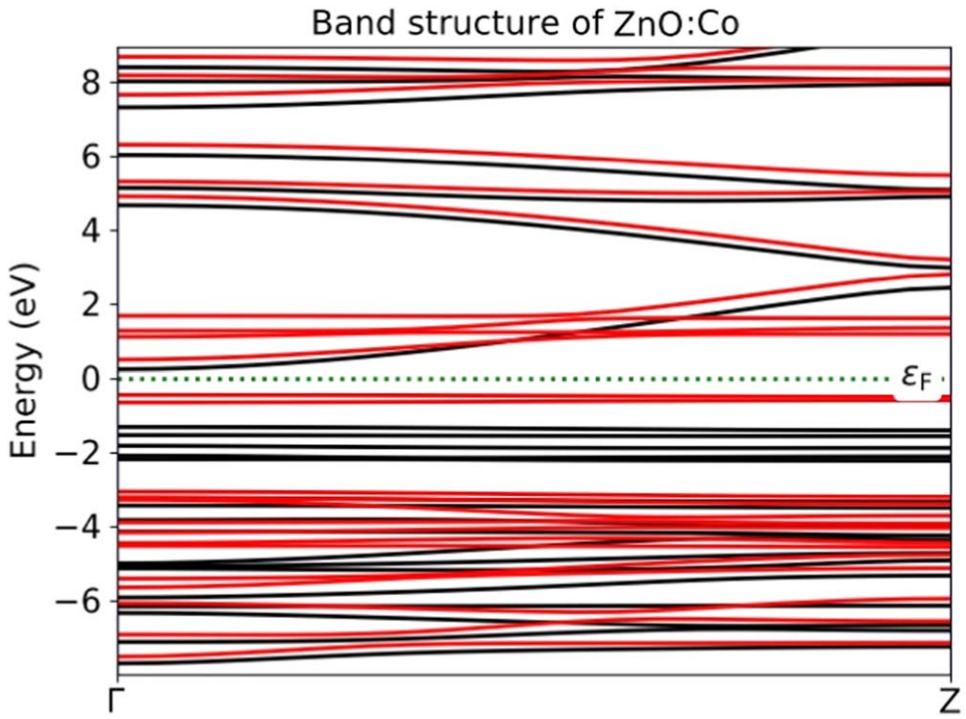

Figure 5. Spin-polarized band structures for Co-doped ZnO 8-atom supercell with LSDA + U. The red and black bands describe the down- and up-spin states.

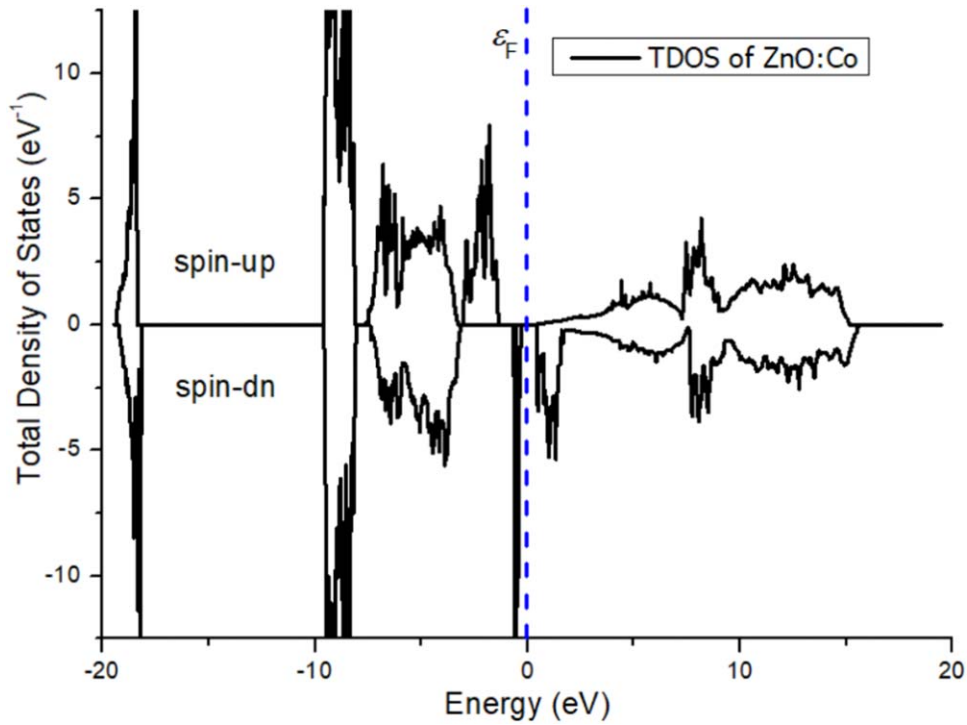

Figure 6. Spin polarized TDOS for Co-doped ZnO 8-atom supercell with LSDA + U.

The first-principles calculated band gap results of Cr-ZnO are given in table 2. Systematic analysis of the electronic properties shows that Cr- and Co-ZnO systems are metallic and half-metallic FM materials.

3.4. Magnetic properties of Zn(Co, Cr)O

Magnetic properties (total and local magnetic moments, FM, and AFM behaviors of ZnO:(Co,Cr) were investigated from Mulliken population analysis based on the DFT-LSDA + U approach.

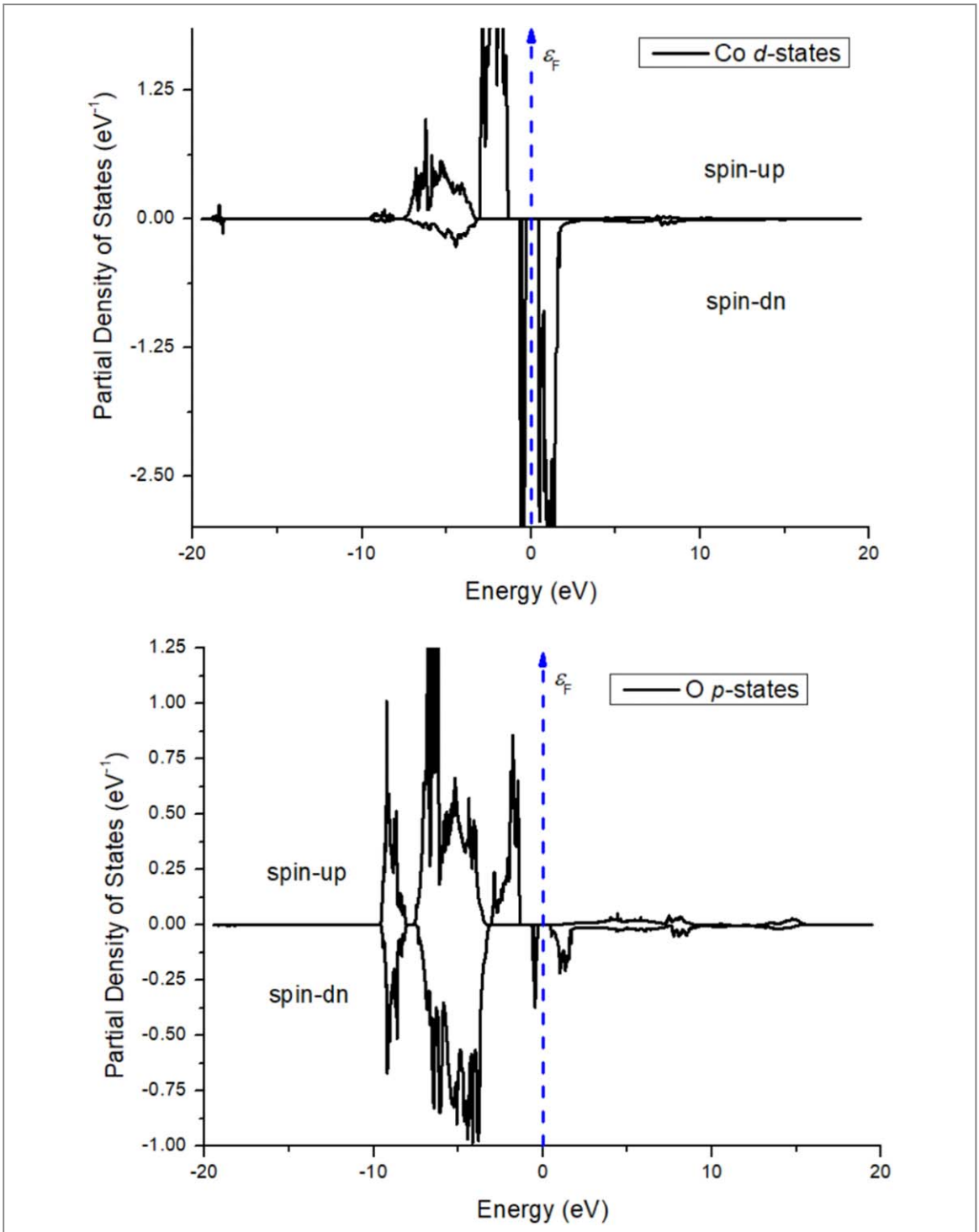

Figure 7. Spin-polarized PDOS diagrams for ZnO:Co with LSDA + U.

The first-principles obtained spin-polarization views for Co- and Cr-ZnO 16-atom systems are present in figure 11. The green arrows describe the significant values of magnetic moments.

In the case of Co-ZnO, the computed magnetic moment of this supercell is ~ 3.0 μ_B and obtained results very close to the result of [43]. The local magnetic moment of cobalt is ~ 2.9 μ_B. The significant positive contribution to the magnetization from Co *d*-orbitals (~2.5 μ_B), the negative contribution (~ 0.7 μ_B) from one zinc atom, which is chemically bonded with Co-O-Zn scheme and shown in rectangle in figure 11. The ~ 0.4 μ_B magnetic moment comes from three oxygen which are chemically bonded with dopants. The insignificant − 0.1 μ_B and significant 0.7 μ_B from other Zn and O atoms, respectively. The computed magnetic moment of ZnO:Cr is ~ 4.0 μ_B, which our result is in good agreement with [34, 44]. From first-principles simulation the chromium local moment of Cr and there are neighboring estimated: ~4.2 μ_B from one Cr (main contribution from *d*-states: ~ 3.4 μ_B), negligible contribution by host atoms. The negative contribution to the magnetization become by one

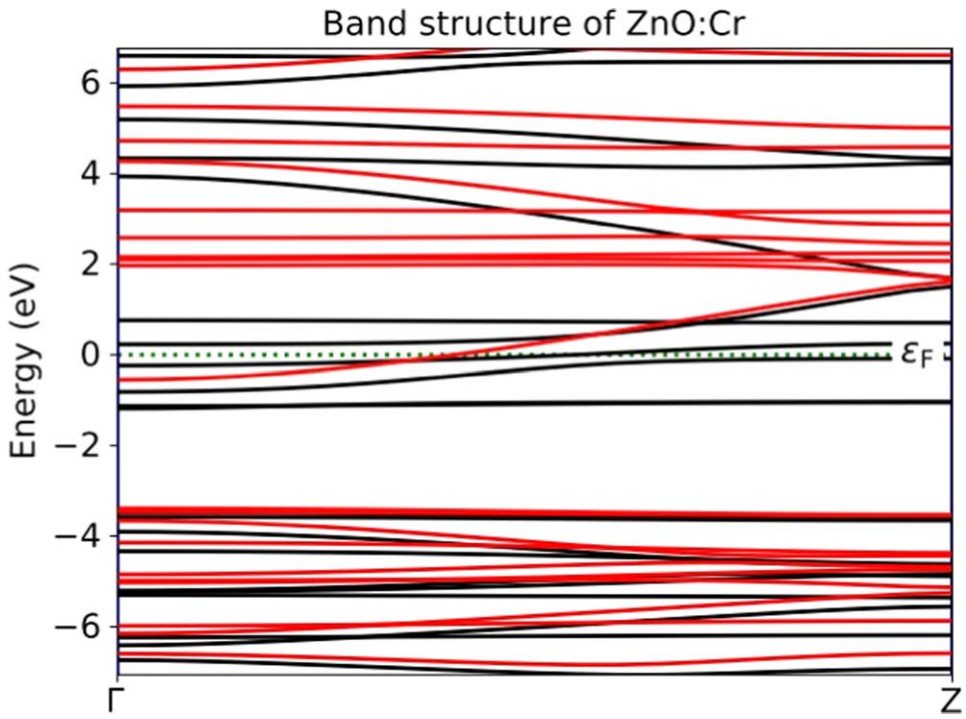

Figure 8. Spin-polarized band structures for Cr-doped ZnO 8-atom supercell with LSDA + U. The red and black bands describe the down- and up-spin states.

Table 1. The band gap results for different Co-ZnO.

Supercells	x [%]	Band gap [eV]	
		Spin-up	Spin-down
$Zn_6Co_2O_8$	25	0	0
$Zn_{14}Co_2O_{16}$	12.5	2.1	0.29
$Zn_{22}Co_2O_{24}$	8.3	2.6	1.5
$Zn_{30}Co_2O_{32}$	6.25	1.2	0.34
$Zn_{46}Co_2O_{48}$	4.16	2.9	1.75
$Zn_{62}Co_2O_{64}$	3.125	2.93	1.64
$Zn_{94}Co_2O_{96}$	2	3	1.8

zinc and one oxygen atom neighboring and the chemical bonding with the dopant. Some structure atoms located in the vicinity of dopants weaken or strengthen the total magnetization of Cr-ZnO supercell with insignificant contributions.

Tables 3 and 4 show the M-M bond lengths, the obtained total energies of ferromagnetic (FM) and antiferromagnetic (AFM) phases, and total energy differences between both alignments (ΔE) for ZnO:M (M = Co, Cr) supercell structures using LSDA + U approach.

In tables 3 and 4, the negative value of energy difference between AFM and FM states is negligible. The first-principles results for total energies for both Co- and Cr-doped ZnO systems show that the FM state is more stable than AFM state.

3.5. Defect formation energies and Curie temperatures of ZnO:(Co, Cr)

The stability of defected systems defined by the defect formation energy of the structure. Defect formation energy simulations were carried out for different large size supercell structures (which FM phase more stable) with different concentrations of impurity atoms.

Defect formation energy of M^{2+}-ZnO systems can be calculated by the formula [45]

$$E_{f.} = \frac{1}{N}[E_{tot.}(Zn_{1-x}M_xO) - E_{tot.}(ZnO) + n \cdot (\mu_{Zn} - \mu_M)] \quad (3)$$

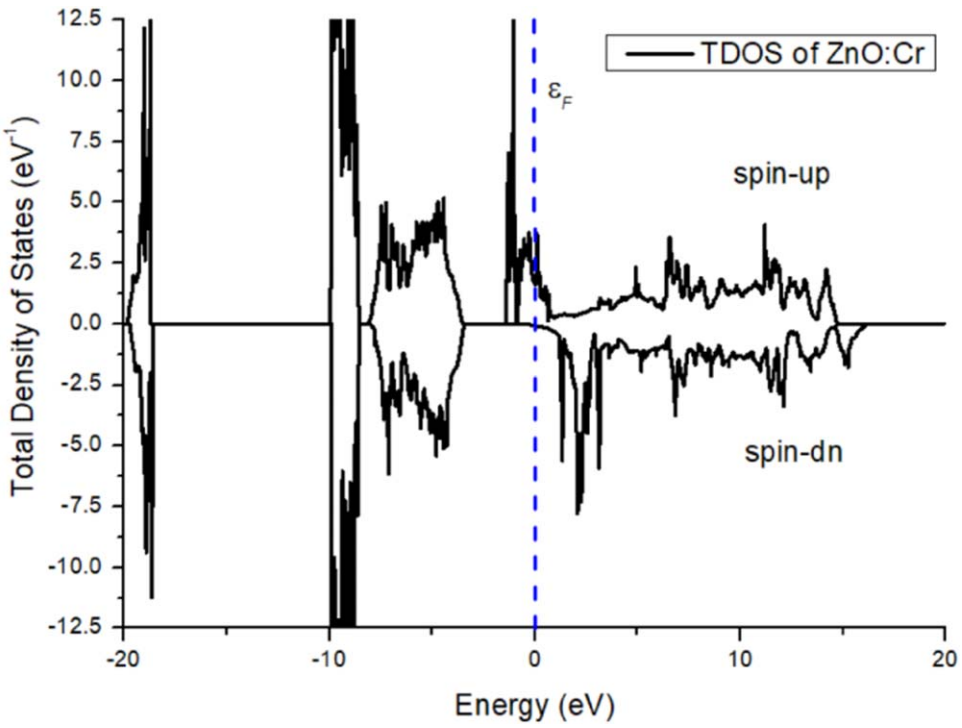

Figure 9. Spin-polarized TDOS for Cr-doped ZnO 8-atom supercell with LSDA + U.

where N is the number of atoms in the structure, $E_{tot.}(Zn_{1-x}M_xO)$ and $E_{tot.}(ZnO)$ are the total energies of doped and undoped supercell structures, having the same dimension, respectively. In formula (1) n and μ are the number of dopants and the chemical potentials of corresponding atoms.

The Curie temperatures of $Co_xZn_{1-x}O$ and $Cr_xZn_{1-x}O$ ($x = 2.08\%$, 3.125%, 4.16%, 6.25%, 8.3%, 12.5% and 25%) different size supercell structures were calculated by Mean Field Approximation (MFA) [45]

$$T_C = \frac{2}{3}\frac{\Delta E}{kx}, \tag{4}$$

where k and x are the Boltzmann constant and concentration of impurity, respectively.

The defect formation energies and the Curie temperatures are estimated for $Zn_{1-x}M_xO$ (M=Co, Cr) supercell structures and tabulated in tables 5 and 6.

Tables 5 and 6 show that the obtained values of defect energies are positive for ZnO:(Co,Cr) systems with concentrations of dopants, indicating that it is hard to incorporate cobalt or chromium into ZnO. The systematic analysis of the stability of the FM phase in ZnO DMSs shows that $Co_xZn_{1-x}O$ compounds are half-metallic and $Cr_xZn_{1-x}O$ systems are metallic materials. The obtained results for Cr-doped ZnO 128- and 192-atom supercell systems show the magnetic properties of higher Curie temperature ferromagnetic materials. We found that the Curie temperatures decrease and increase with the decreasing of impurity atom concentrations for $Zn_{1-x}Co_xO$ and $Zn_{1-x}Cr_xO$ defected materials. Our results indicate that the both Co- and Cr-doped ZnO are suitable materials for spin-based devices.

4. Conclusion

We have carried out a systematic analysis of the electronic and magnetic properties of $Co_xZn_{1-x}O$ and $Cr_xZn_{1-x}O$ with 2.08%, 3.125%, 4.16%, 6.25%, 8.3%, 12.5% and 25% impurity atom concentrations, using the LSDA + U approach based on DFT formalism. Employing Hubbard energies enable us to find an accurate energy gap for investigated diluted magnetic compounds and study of magnetic properties of these systems. The magnetic and electronic properties of $Zn_{1-x}Co_xO$ and $Zn_{1-x}Cr_xO$ doped systems for $0.02 \leqslant x \leqslant 0.25$ were investigated. The DOS calculations show that when the ZnO-doped by Co and Cr ions, the M 3*d*-states are situated in the energy gap area. From first-principles results, we observed Co- and Cr-doped ZnO present magnetic properties and the total magnetization of investigated systems is mainly derived from the dopant 3*d*-states.

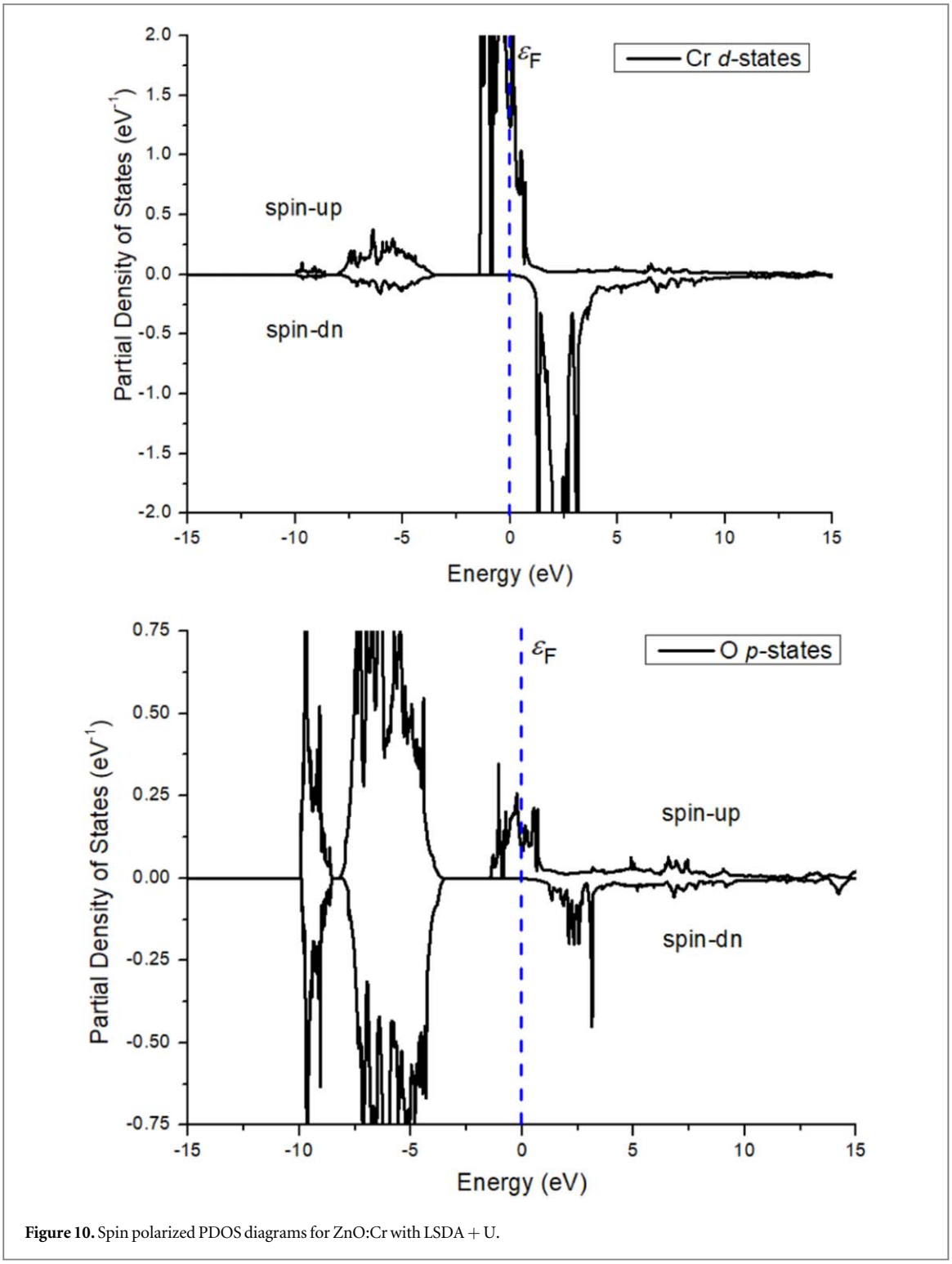

Figure 10. Spin polarized PDOS diagrams for ZnO:Cr with LSDA + U.

The introduction of M=Co, Cr atoms in ZnO lead to the magnetization of structure due to *p-d* hybridization between the 3*d*-states of metal and 2*p* states of oxygen. The Zn(Co,Cr) substitutions induce local moments of ~2.9 and ~4.2 μ_B, and $(Co,Cr)_xZn_{1-x}O$ materials exhibit half-metallic and metallic nature and these materials are potential DMS for spin-based devices.

The analysis of ferromagnetic and antiferromagnetic phases show that depending on concentrations of dopants and their positions these phases were the ground state for both $Co_xZn_{1-x}O$ and $Cr_xZn_{1-x}O$ supercell structures.

Our first-principles results predicted Cr-doped ZnO is one of the prominent ferromagnetic materials that can be used as a high temperature sensor because it is stable at high temperature and exhibits high Curie temperature. Co-doped ZnO exhibits paramagnetic character and it is useful material for magneto-optical

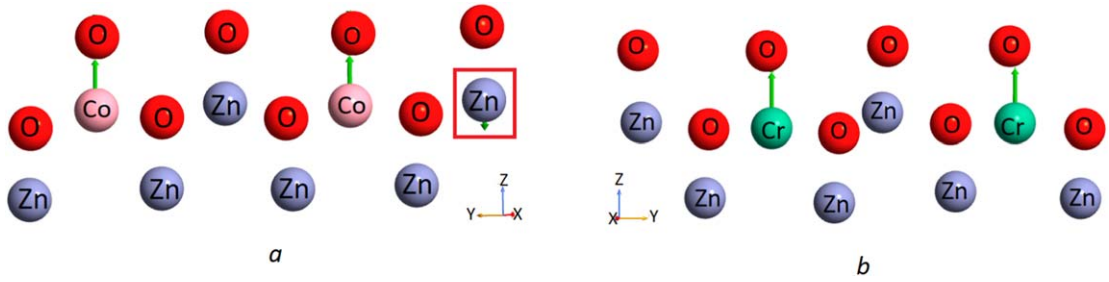

Figure 11. Spin-polarization views for Co- and Cr-ZnO 16-atom supercell systems. The values of magnetic moments are described by green arrows.

Table 2. The calculated band gap results for different Cr-ZnO.

Supercells	x [%]	Band gap [eV]	
		Spin-up	Spin-down
$Zn_6Cr_2O_8$	25	0	0
$Zn_{14}Cr_2O_{16}$	12.5	0	0
$Zn_{22}Cr_2O_{24}$	6.25	0, 1	0
$Zn_{30}Cr_2O_{32}$	8.33	0.4	3
$Zn_{46}Cr_2O_{48}$	4.16	0	0
$Zn_{62}Cr_2O_{64}$	3.125	0	0
$Zn_{94}Cr_2O_{96}$	2.083	0	0

Table 3. The Co-Co distances and the total energy differences between AFM and FM phases for different ZnO:Co.

Supercells	$d_{Co\text{-}Co}$ [Å]	E_{AFM} [eV]	E_{FM} [eV]	$\Delta E/2$ [eV]
$Zn_{14}Co_2O_{16}$	8.60	−30905.80826	−30905.80776	−0.00025
$Zn_{22}Co_2O_{24}$	6.14	−46982.49351	−46982.49291	−0.0003
$Zn_{30}Co_2O_{32}$	10.05	−63114.88241	−63114.88251	0.00005
$Zn_{46}Co_2O_{48}$	8.15	−94936.25267	−94936.25273	0.00003
$Zn_{62}Co_2O_{64}$	5.53	−127479.17867	−127479.17891	0.00012
$Zn_{94}Co_2O_{96}$	6.42	−191871.68194	−191871.68164	−0.00015

Table 4. The Cr–Cr distances and the total energy differences between AFM and FM phases for different ZnO:Cr.

Supercells	$d_{Cr\text{-}Cr}$ [Å]	E_{AFM} [eV]	E_{FM} [eV]	$\Delta E/2$ [eV]
$Zn_{22}Cr_2O_{24}$	6.14	−46094.94912	−46094.95077	0.000825
$Zn_{30}Cr_2O_{32}$	10.05	−62229.49456	−62229.48515	−0.004705
$Zn_{46}Cr_2O_{48}$	8.15	−94395.90584	−94395.90645	0.000305
$Zn_{62}Cr_2O_{64}$	5.53	−126590.72538	−126590.76764	0.02113
$Zn_{94}Cr_2O_{96}$	6.42	−190983.82584	−190983.85085	0.012501

Table 5. The results of defect formation energies and the curie temperatures of $Co_xZn_{1-x}O$.

Supercells	x, [%]	E_f.[eV]	T_C [K]
$Zn_{30}Co_2O_{32}$	6.25	20.25	6.19
$Zn_{46}Co_2O_{48}$	4.16	13.98	5.57
$Zn_{62}Co_2O_{64}$	3.125	10.41	29.7

Table 6. The results of defect formation energies and the Curie temperatures of $Cr_xZn_{1-x}O$.

Supercells	x, [%]	E_f[eV]	T_C [K]
$Zn_{22}Cr_2O_{24}$	8.33	46	76.5
$Zn_{46}Cr_2O_{48}$	4.166	23.17	56.6
$Zn_{62}Cr_2O_{64}$	3.125	17.30	5231
$Zn_{94}Cr_2O_{96}$	2.083	11.76	4643

devices. The results of this paper may be valuable for alloyed and doped Zn-based applications in electronic, optoelectronic, nanoelectronic, and spintronic devices in the future.

Data availability statement

The data cannot be made publicly available upon publication because no suitable repository exists for hosting data in this field of study. The data that support the findings of this study are available upon reasonable request from the authors.

Author statement

All authors have participated in this research work, and they are aware and accepting this submission.

Declaration of competing interest

The authors do not have any conflict of interest to declare.

ORCID iDs

V N Jafarova https://orcid.org/0000-0002-0643-1464

References

[1] Dong C, Persson C, Vayssieres L, Augustsson A, Schmitt T, Mattesini M, Ahuja R, Chang C L and Guo J-H 2004 Electronic structure of nanostructured ZnO from x-ray absorption and emission spectroscopy and the local density approximation *Phys. Rev.* **70** 195325
[2] Huang M H, Mao S, Feick H, Yan H, Wu Y, Kind H, Weber E, Russo R and Yang P 2001 Room-temperature ultraviolet nanowire nanolasers *Science* **292** 1897–9
[3] Jafarova V N and Orudzhev G S 2021 Structural and electronic properties of ZnO: A first-principles density-functional theory study within LDA(GGA) and LDA(GGA) + U methods *Solid State Commun.* **325** 114166
[4] Jafarova V N 2022 Ab-initio calculation of structural and electronic properties of ZnO and ZnSe compounds with wurtzite structure *Int. J. Mod. Phys.* B **36** 2250156
[5] Janotti A and Van de Walle C G 2009 Fundamentals of zinc oxide as a semiconductor *Rep. Prog. Phys.* **72** 126501
[6] Pearton S J, Norton D P, Ip K, Heo Y W and Steiner T 2005 RETRACTED: recent progress in processing and properties of ZnO *Prog. Mater. Sci.* **50** 293–340
[7] Tsukazaki A *et al* 2005 Repeated temperature modulation epitaxy for p-type doping and light-emitting diode based on ZnO *Nat. Mater.* **4** 42–6
[8] Repins I, Contreras M A, Egaas B, De Hart C, Scharf J, Perkins C L, To B and Noufi R 2008 19.9%-Efficient ZnO/CdS/$CuInGaSe_2$ solar cell with 81.2% fill factor *Prog. Photovolt. Res. Appl.* **16** 235–9
[9] Morkoç H and Özgür Ü 2009 Zinc oxide: fundamentals *Materials and Device Technology* **131** 1–76
[10] Klingshirn C 2007 ZnO: from basics towards applications *Phys. Status Solidi* B **244** 3027–73
[11] Guo H, Lu N, Dai J, Zeng X C, Wu X and Yang J 2014 Electronic structure engineering in chemically modified ultrathin ZnO nanofilms via a built-in heterointerface *RSC Adv.* **4** 18718–23
[12] Spaldin N A 2004 Search for ferromagnetism in transition-metal-doped piezoelectric ZnO *Phys. Rev.* B **69** 125201
[13] Rode K, Anane A, Mattana R, Contour J P, Durand O and Bourgeois R L 2003 Magnetic semiconductors based on cobalt substituted ZnO *J. Appl. Phys.* **93** 7676–8
[14] Cho Y M, Choo W K, Kim H, Kim D and Ihm Y 2002 Effects of rapid thermal annealing on the ferromagnetic properties of sputtered $Zn_{1-x}(Co_{0.5}Fe_{0.5})_xO$ thin films *Appl. Phys. Lett.* **80** 3358–60
[15] Singhal R K, Dhawan M S, Gaur S K, Dolia S N, Kumar S, Shripathi T, Deshpande U P, Xing Y T, Saitovitch E and Garg K B 2009 Room temperature ferromagnetism in Mn-doped dilute ZnO semiconductor: an electronic structure study using x-ray photoemission *J. Alloys Compd.* **477** 379–85
[16] Wang J, Chen W and Wang M R 2008 Properties analysis of Mn-doped ZnO piezoelectric films *J. Alloys Compd.* **449** 44–7

[17] Satoh I and Kobayashi T 2003 Magnetic and optical properties of novel magnetic semiconductor Cr-Doped ZnO and its application to all oxide p-i-n diode *J. Appl. Surf. Sci.* **216** 603–6
[18] Jafarova V N and Rzayeva S S 2024 First-principles prediction of higher curie temperature, metallic and half-metallic ferromagnetism in $Zn_{1-x}(V_x,Ni_x)O$ systems. *Chin. J. Phys.* **87** 592–607
[19] Ayoub I, Kumar V, Abolhassani R, Sehgal R, Sharma V, Sehgal R, Swart and H C and Mishra Y K 2022 Advances in ZnO: manipulation of defects for enhancing their technological potentials *Nanotechnol. Rev.* **11** 575–619
[20] González-Garnica M *et al* 2021 One dimensional Au-ZnO hybrid nanostructures based CO2 detection: growth mechanism and role of the seed layer on sensing performance *Sens. Actuators B Chem.* **337** 129765
[21] Shinde R, Yamijala S S R K C and Wong B M 2021 *J. Phys. Condens. Matter* **33** 115501
[22] Morozova N K and Abbasov I I 2023 Luminescence due to oxygen at structural defects in A_2B_6 crystals *Ind. J. Phys.* **98** 1–10
[23] Cococcioni M and de Gironcoli S 2005 Linear response approach to the calculation of the effective interaction parameters in the LDA + U method *Phys. Rev.* B **71** 035105
[24] Farooq R, Mahmood T and Anwar A W 2016 First-principles calculation of electronic and optical properties of graphene like ZnO (G-ZnO) *Superlattice. Microst.* **90** 165–9
[25] Zhang H, Lu S, Xu W and Yuan F 2014 First-principles study of Si atoms adsorbed on ZnO (0001) surface and the effect on electronic and optical properties *Surf. Sci.* **625** 30–6
[26] Yaakob M K *et al* 2014 First principles LDA + U calculations for ZnO materials *Integrated Ferroelectrics Int. J.* **155** 15–22
[27] Jafarova V N 2023 High Curie temperature and half-metallic ferromagnetism in Cr- and V-doped ZnSe in wurtzite phase: first-principles study *Solid State Commun.* **369** 115197
[28] Sato K and Katayama-Yoshida H 2001 Ferromagnetism in a transition metal atom doped ZnO *Physica* E **10** 251–5
[29] Krishnan K M, Shutthanandan V S, Roberts B K and Pakhomov A B 2005 Ferromagnetic Cr-doped ZnO for spin electronics via magnetron sputtering *J. Appl. Phys.* **97** 10D310
[30] Li H, Sang J P, Mei F, Ren F, Zhang L and Liu C 2007 Observation of ferromagnetism at room temperature for Cr^+ ions implanted ZnO thin films *Appl. Surf. Sci.* **253** 8524–9
[31] Venkatesan M, Fitzgerald C B, Lunney J G and Coey J M D 2004 Anisotropic ferromagnetism in substituted zinc oxide *Phys. Rev. Lett.* **93** 177206
[32] Ueda K, Tabata H and Kawai T 2001 Magnetic and electric properties of transition-metal-doped ZnO films *Appl. Phys. Lett.* **79** 988
[33] Najim M, Sharma V K and Varma G D 2012 Effect of annealing atmosphere on the optical and magnetic properties of Cr Doped ZnO Samples *J. Spintron. Magn. Nanomater.* **1** 109–12
[34] Li L Y, Li H, Luo X G, Zhang X, Wang W H, Cheng Y and Song Q G 2008 Ferromagnetism in polycrystalline Cr-doped ZnO films: experiment and theory *Solid State Commun.* **146** 420–4
[35] Roberts B K, Pakhomov A B, Shutthanandan V S and Krishnan K M 2005 *J. Appl. Phys.* **97** 10D310
[36] Martin F and Matthias S 1999 *Ab initio* pseudopotentials for electronic structure calculations of poly-atomic systems using density-functional theory *Comput. Phys. Commun.* **119** 67–79
[37] Perdew J and Zunger A 1981 Self-interaction correction to density-functional approximations for many-electron systems *Phys. Rev.* B **23** 5048–79
[38] Monkhorst H J and Pack J D 1976 Special points for brillouin-zone integrations *Phys. Rev.* B **13** 5188–92
[39] Dudarev S L, Botton G A, Savrasov S Y, Humphreys C J and Sutton A P 1998 Electron-energy-loss spectra and the structural stability of nickel oxide: An LSDA + U study *Phys. Rev.* B **57** 1505
[40] Liechtenstein A I, Anisimov V I and Zaanen J 1995 Density-functional theory and strong interactions: orbital ordering in Mott-Hubbard insulators *Phys. Rev.* B **52** R5467
[41] Wyckoff R W G 1963 *Crystal Structures* **1** 85 https://worldcat.org/title/31183170
[42] North S C, Jorgensen K R, Pricetolstoy J and Wilson A K 2023 Population analysis and the effects of Gaussian basis set quality and quantum mechanical approach: main group through heavy element species *Front. Chem.* **11** 1152500
[43] Sharma Y, Anand V and Heera P 2023 *Ab initio* study of structural and magnetic properties of cobalt doped zinc oxide *J. Condens. Matter.* **1** 48–51
[44] Jia X, Qin M and Yang W 2011 Magnetism in Cr doped ZnO: density-functional theory studies *J. Magn. Magn. Mater.* **323** 1423–7
[45] Jafarova V N, Mamedov N T and Musaev M A 2023 High curie temperature and half-metallic ferromagnetism in ZnSe:Co,Ni with wurtzite structure: first-principles study *Phys. Status Solidi* B **260** 2200360